



## Shiṣr 043 (IIIAB medium octahedrite): The first iron meteorite from the Oman desert

A. AL-KATHIRI<sup>1,2\*</sup>, B. A. HOFMANN<sup>3</sup>, E. GNOS<sup>1</sup>, O. EUGSTER<sup>4</sup>, K. C. WELTEN<sup>5</sup>,  
and U. KRÄHENBÜHL<sup>6</sup>

<sup>1</sup>Institut für Geologie, Universität Bern, Baltzerstrasse 1, CH-3012 Bern, Switzerland

<sup>2</sup>Directorate General of Commerce and Industry, Ministry of Commerce and Industry, Salalah, Sultanate of Oman

<sup>3</sup>Naturhistorisches Museum der Burgergemeinde Bern, Bernastrasse 15, CH-3005 Bern, Switzerland

<sup>4</sup>Physikalisches Institut, Abteilung für Weltraumforschung und Planetologie, Universität Bern, Sidlerstrasse 5, CH-3012 Bern, Switzerland

<sup>5</sup>Space Science Laboratory, 7 Gauss Way, University of California—Berkeley, Berkeley, California, 94720–7450, USA

<sup>6</sup>Departement für Chemie und Biochemie, Universität Bern, Freiestrasse 3, CH-3012 Bern, Switzerland

\*Corresponding author. E-mail: alikath@geo.unibe.ch

(Received 15 March 2006; revision accepted 10 May 2006)

**Abstract**—The iron meteorite Shiṣr 043 is a single mass of 8267 g found in the south Oman desert 42 km NE of the Shiṣr village. It is the first iron identified among the >1400 individual meteorites reported from Oman. The meteorite is a slightly elongated mass showing only minor rusting, a partially smooth and partially rough surface with octahedral cleavage, and a partially preserved metallic fusion crust typically 0.75 mm thick.

The undeformed Widmanstätten pattern with a mean kamacite bandwidth of  $1.0 \pm 0.1$  mm ( $n = 97$ ) indicates structural classification as a medium octahedrite. From the bulk composition, Ni = 8.06 wt%, Ga = 18.8 ppm, Ge = 37.25 ppm, and Ir = 3.92 ppm, the meteorite is classified as IIIAB, the most common group of iron meteorites. The cosmic-ray exposure (CRE) age based on <sup>3</sup>He, <sup>21</sup>Ne, <sup>38</sup>Ar concentrations and <sup>10</sup>Be–<sup>21</sup>Ne, <sup>26</sup>Al–<sup>21</sup>Ne, and <sup>36</sup>Cl–<sup>36</sup>Ar ratios is  $290 \pm 20$  Ma. This age falls within the range observed for type IIIAB iron meteorites, but does not coincide with the main cluster. The cosmogenic noble gas and radionuclide data indicate that Shiṣr 043 had a relatively small pre-atmospheric mass. The low degree of weathering is consistent with a young terrestrial age of <10,000 years based on the saturated <sup>41</sup>Ca concentration. Shiṣr 043 is not paired with any of the other eight known iron meteorites from the Arabian Peninsula.

### INTRODUCTION

Iron meteorites comprise about 5% of falls (Grady 2000; McSween 1999; Norton 2002) but are underrepresented in hot and cold desert finds. Irons represent only 1.3% of Antarctic finds (Bevan et al. 1998) and 0.4% in the Dar al Gani area, Libya (Schlüter et al. 2002). Despite of the large number of meteorite finds in Oman since 1999 and the relatively high fraction of rare types such as lunar and Martian achondrites (Grossman 2000; Grossman and Zipfel 2001; Russell et al. 2002, 2003, 2004, 2005), Shiṣr 043 is the only iron meteorite among >1400 finds reported from Oman during 2000–2005 (0.07% of all finds). Shiṣr 043 was recovered during a joint Omani-Swiss meteorite search program initiated in 2001, which involves geologists from Bern, Switzerland (University of Bern and Natural History Museum Bern), and the Ministry of Commerce and Industry, Sultanate of Oman. During this search program, samples from more than 260

individual meteorite falls were recovered (Al-Kathiri et al. 2005). A closer characterization of Shiṣr 043 was initiated because of the underrepresentation of irons in Oman while several irons are known from Saudi Arabia; therefore, testing for possible pairing appeared important.

### SAMPLES AND METHODS

After recovery, the iron mass was cleaned with pressurized air, rust was fixed with cyanomethacrylate, and two parallel cuts were made. The end piece (90 × 50 × 10 mm, 326.1 g) was etched while subsamples from the slice (95 × 50 × 6 mm, 172.0 g) were used for subsequent analyses. Weathering-related materials were collected immediately adherent to the meteorite (coarse oxide flakes, fine oxide flakes, and magnetic and non-magnetic soil fraction). In addition, two types of bulk soil samples were collected: a) a sample of soil from under the meteorite (SUM), and b) a

reference soil sample (RSS) taken from the top 5 cm at a distance of about 10 m from the meteorite. Soil samples were sieved to obtain the fractions <0.15 mm which was analyzed.

Chemical analyses of fresh metal were performed at several laboratories using the following methods: inductively coupled plasma emission spectroscopy (ICP-OES) was performed at the Department for Chemistry and Biochemistry, University of Bern, Switzerland; atomic absorption spectroscopy was performed at the University of California, Berkeley; instrumental neutron activation analysis (INAA) data were obtained commercially from Activation Laboratories Ltd., Ancaster, Ontario, Canada (using Odessa iron meteorite and NBS 809B steel as internal standards); X-ray fluorescence (XRF) analyses were obtained nondestructively on polished sections at the Institute of Geology, University of Fribourg, Switzerland, using a Philips PW 2400 spectrometer and the semiquantitative program Uniquant 5.

A freshly cut and polished surface of the meteorite was etched with nitric acid (3% in ethanol) to develop the Widmanstätten pattern (Fig. 1a). The average kamacite bandwidth was measured using the software “NIH image” on digital images obtained from the etched section.

Noble gas analyses of a sample of 52.45 mg were performed at the Physics Institute of the University of Bern. The sample was heated in vacuum at 90 °C for several days in the storage arm of the extraction system to reduce adsorbed atmospheric gases. The noble gases were extracted by RF-heating in a single step at 1700 °C in a Mo crucible. Completeness of the gas release was checked by adding a final step at 1740 °C. The mass spectrometric analyses and background corrections were performed according to the description by Eugster et al. (1993) using our system B. The following blanks were subtracted (units of  $10^{-8}\text{cm}^3\text{STP/g}$ ):  $^3\text{He} < 0.00004$ ,  $^4\text{He} = 0.02$ ,  $^{20}\text{Ne} = 0.0008$ ,  $^{40}\text{Ar} = 0.4$ . The errors given correspond to a 95% confidence level.

A sample of ~98 mg was ultrasonically agitated in 0.2 N HCl to dissolve possible troilite inclusions. The purified metal sample of 97.7 mg was dissolved in 1.5 N  $\text{HNO}_3$ , along with a carrier solution containing Be, Al, Cl, Ca, and Mn. After taking an aliquot for chemical analysis by atomic absorption spectrometry, Cl was isolated as AgCl. Be, Al, and Ca were separated by anion exchange chromatography, acetylacetone solvent extraction, and cation exchange chromatography techniques described in Lavielle et al. (1999). The separated fractions of Be, Al, Cl, and Ca were further purified and converted to  $\text{BeO}$ ,  $\text{Al}_2\text{O}_3$ , AgCl, and  $\text{CaF}_2$  for AMS measurements. The ratios of  $^{10}\text{Be}/\text{Be}$ ,  $^{26}\text{Al}/\text{Al}$ , and  $^{41}\text{Ca}/\text{Ca}$  were determined using the Lawrence Livermore National Laboratory AMS facility (Roberts et al. 1997). After making corrections for background and chemical blanks, the measured ratios were normalized to AMS standards (Nishiizumi 2004; Nishiizumi et al. 1984, 2000; Sharma et al. 1990).

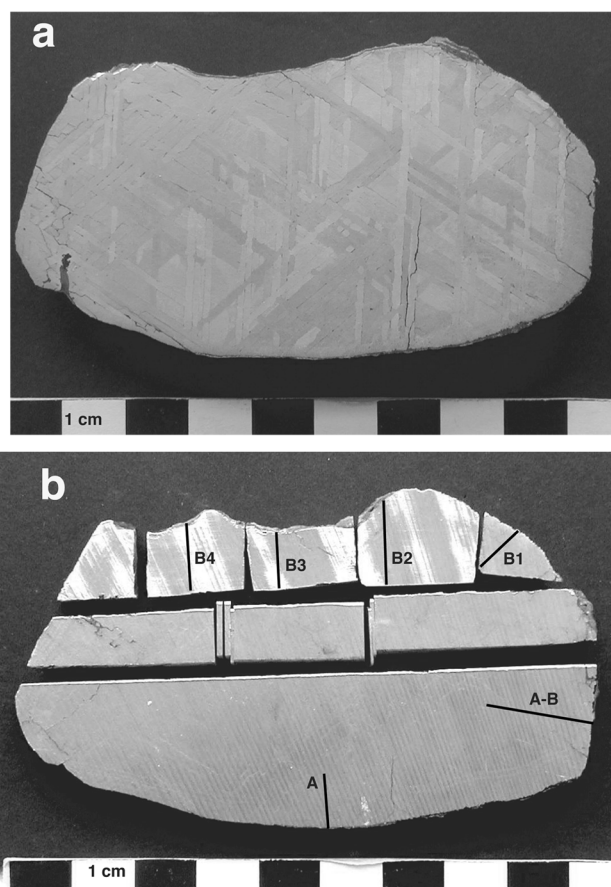


Fig. 1. Cut slabs. a) Etched end-piece displaying typical Widmanstätten pattern. Fracturing parallel to kamacite bands is common. A partially corroded troilite inclusion is at lower left. Note the heat-affected zone at the lower edge of the sample. b) A section indicating the position of microhardness profiles shown in Fig. 4. All samples for analyses were obtained from the central part of the narrow bar. Striation is a cutting artifact.

The microhardness of the meteorite was measured on polished sections using a reflected light microscope (Leitz Durimet 2) equipped with a Vickers hardness probe and a 100 g weight. Six profiles were measured perpendicular to the different natural surface types (Fig. 1b). In order to check the quality of our hardness measurements, hardness profiles were measured on a polished standard metal with a known hardness of HV 585 (100 g wt.) and on two meteorites with homogeneous hardness, the IA Odessa and IIB São Julião de Moreira (Buchwald 1975).

Sieved soil samples were analyzed without further treatment by ICP-OES following aqua regia extraction (Activation Laboratories Ltd., Ancaster, Ontario, Canada). For bulk chemistry, weathered oxide crust adherent to the meteorite, magnetic and nonmagnetic soil fraction, and SUM and RSS samples were ground in an agate mill and 5 g of each sample were submitted for analysis by ICP-MS to Activation Laboratories Ltd., Ancaster, Ontario, Canada.

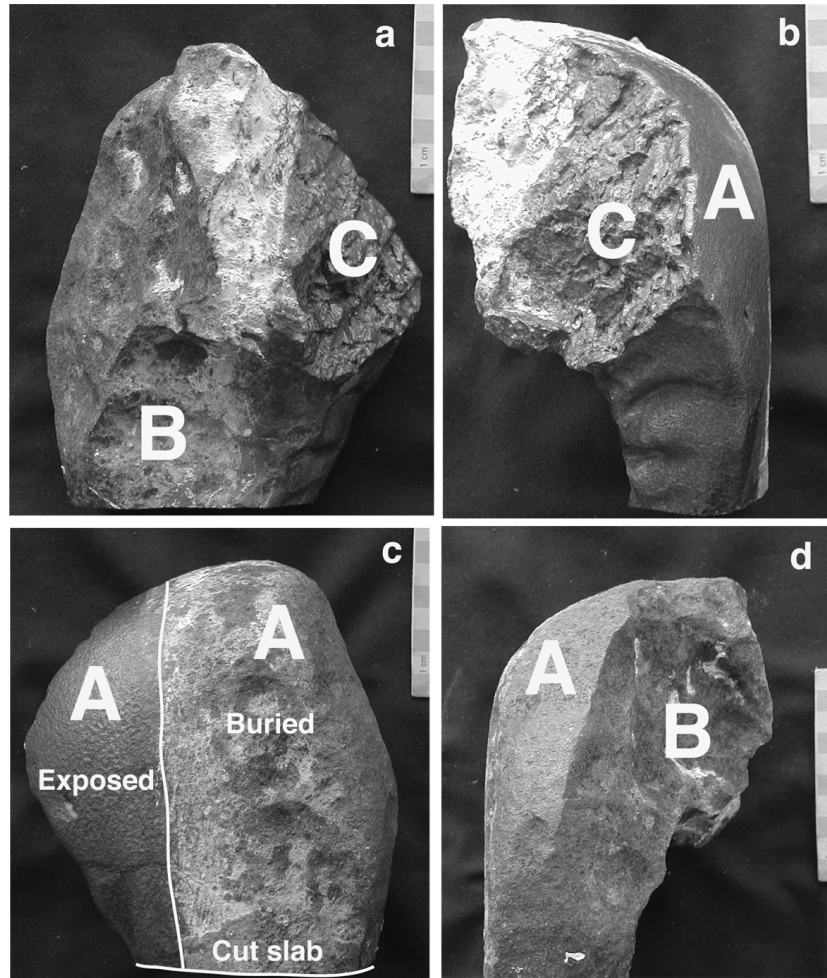


Fig. 2. Different views of Shiṣr 043 illustrating the differences in surface types (A–C). Note that about two-thirds of the meteorite was buried in the soil as visible in (a) and (c). The line at the bottom of (c) indicates the location of the etched slab which was also used for hardness measurements.

## RESULTS

### Field Observations and Macroscopic Description of the Surface

Shiṣr 043 was found on January 21, 2003, in the south Omani desert (18°35.546'N, 53°48.748'E), 42 km NE of Shiṣr village. The meteorite was found on subrecent alluvial fan material of Quaternary, 1.6 Ma to present age (Chevrel et al. 1992). The sediments largely consist of fine-grained silty to sandy material with some unsorted but well-rounded clasts of hard bioclastic limestone derived from the Dammam Formation of Eocene age (Chevrel et al. 1992). Few quartz geodes are locally found likely to be derived from the Late Paleocene-Eocene Umm er Radhuma Formation, which is mainly composed of carbonates.

About two-thirds of the meteorite was buried in the soil when it was found (Fig. 2c). The exposed part appears smooth and shiny with a dark brown color. The buried part is covered

by reddish brown, flaky rust, and locally by a calcite crust, especially in the upper 3 cm below the surface.

Shiṣr 043 is of irregular shape with maximum dimensions of  $19 \times 14.5 \times 5$ –10 cm. The single mass had a total weight of 8267 g prior to cutting. An additional 140 g of magnetic oxide was recovered from the immediate surroundings. Three meteorite surface types can be distinguished (Fig. 2): Surface type A dominates the meteorite on several sides. This surface type is smooth and gently curved, covering approximately 60% of the meteorite. Only in one area are regmaglypts visible. The rest of the meteorite has two surfaces with different orientations and characteristics. B is concave with abundant shallow pits 2–5 cm in diameter, and is at least partly covered by metallic fusion crust, specially accumulated at boundaries between surface A and B. Surface C is characterized by octahedral cleavage planes up to 5 cm in size, with octahedral plane orientations corresponding to those of the Widmanstätten pattern in the etched section. The formation of surface types

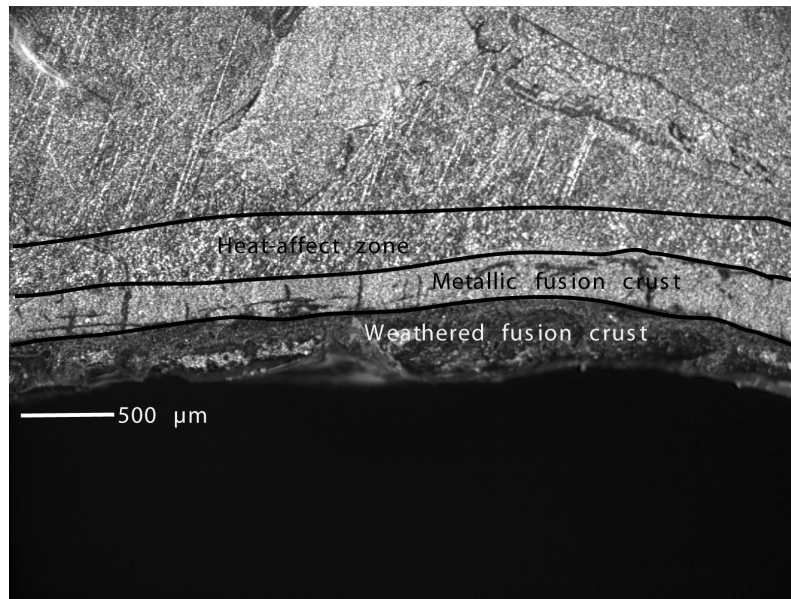


Fig. 3. An image taken under a stereo microscope under oblique illumination showing the different heat-affected zones that formed during the meteorite's atmospheric trajectory. The exterior part of the fusion crust is altered to iron oxides and hydroxides as a result of terrestrial weathering.

A and B could be due to different orientations in flight, or surface B could be formed due to breakup of surface A shortly after entering the Earth's atmosphere. Surface type C clearly results from a late breakup event after which not much ablation occurred. There is no indication on any of the surfaces of the presence of troilite nodules.

### Structure, Mineralogy, and Microhardness

The Widmanstätten pattern is clearly developed after etching (Fig. 1a). The average kamacite bandwidth obtained on undeformed kamacite bands is  $1.0 \pm 0.1$  mm ( $n = 97$ , not corrected for orientation). The taenite lamellae typically are 10–50  $\mu\text{m}$  thick. Only one troilite aggregate of  $1 \times 4$  mm was observed on approximately 88  $\text{cm}^2$  of cut surface, corresponding to 0.045 vol% troilite or  $\sim 0.01$  wt% S. This low S content is consistent with the absence of large troilite nodules anywhere on cut and natural surfaces of the meteorite. There is evidence of fracturing, mainly along the octahedral planes of the Widmanstätten pattern, as seen in Fig. 1a. Neumann bands are abundant.

The meteorite is partially covered by fusion crust reaching a maximum thickness of 1.7 mm (typically up to 0.75 mm) on surface B (Fig. 3). The fusion crust consists of multiple layers of Fe-Ni metal with abundant microspherules of magnetite/wüstite reaching a maximum of 10  $\mu\text{m}$  in diameter. At many places the outermost 0.4 mm of the fusion crust is weathered to iron hydroxides and iron oxides. However, its inner limit is defined by a sharp boundary to the heat-affected zone  $\alpha_2$ .

Beneath the metallic fusion crust, the heat-affected zone  $\alpha_2$  is optically observed in the etched section using medium magnification and oblique illumination (Fig. 3). It is seen as a fine-grained dim rim following the contours of the meteorite and ranges in width from 0.25 mm to 0.4 mm. This zone is known to be caused by a rapid diffusionless transformation of kamacite to unequilibrated serrated iron- $\alpha_2$  under temperature briefly exceeding 750  $^\circ\text{C}$  (Buchwald 1975). Below a depth of 0.75 mm to 4 mm occurs a heat-affect zone not seen optically but recovered by hardness measurements. This zone shows systematic hardness increase with depth resembling the recovery zone as described by Buchwald (1975).

Initial hardness measurements demonstrated that Shiřr 043 is strongly shock-hardened, thus providing the opportunity to investigate depth of heat penetration during atmospheric entry by measuring hardness profiles. Six hardness profiles were subsequently measured (Fig. 1b), one on surface A (profile A), four on surface B (profiles B1 to B4) and one on the area between surface A and B (profile A-B).

Hardness measurements on three fusion crust profiles show an increase of hardness with depth. The average Vickers hardness (HV) at different depths is 361 at 0.02 mm, 378 at 0.05 mm, and  $441 \pm 35$  at 0.1 mm.

Hardness values from the concave surface B1–B4 profiles (Figs. 4a–4d), measured from the surface or from below the fusion crust (profile B1 does not contain fusion crust) to a depth of several mm show:

- a. The first zone of decreased hardness (resembling the heat-affect  $\alpha_2$ ) to a depth of about 0.5 mm reaching a minimum hardness of  $\text{HV } 213 \pm 47$ .

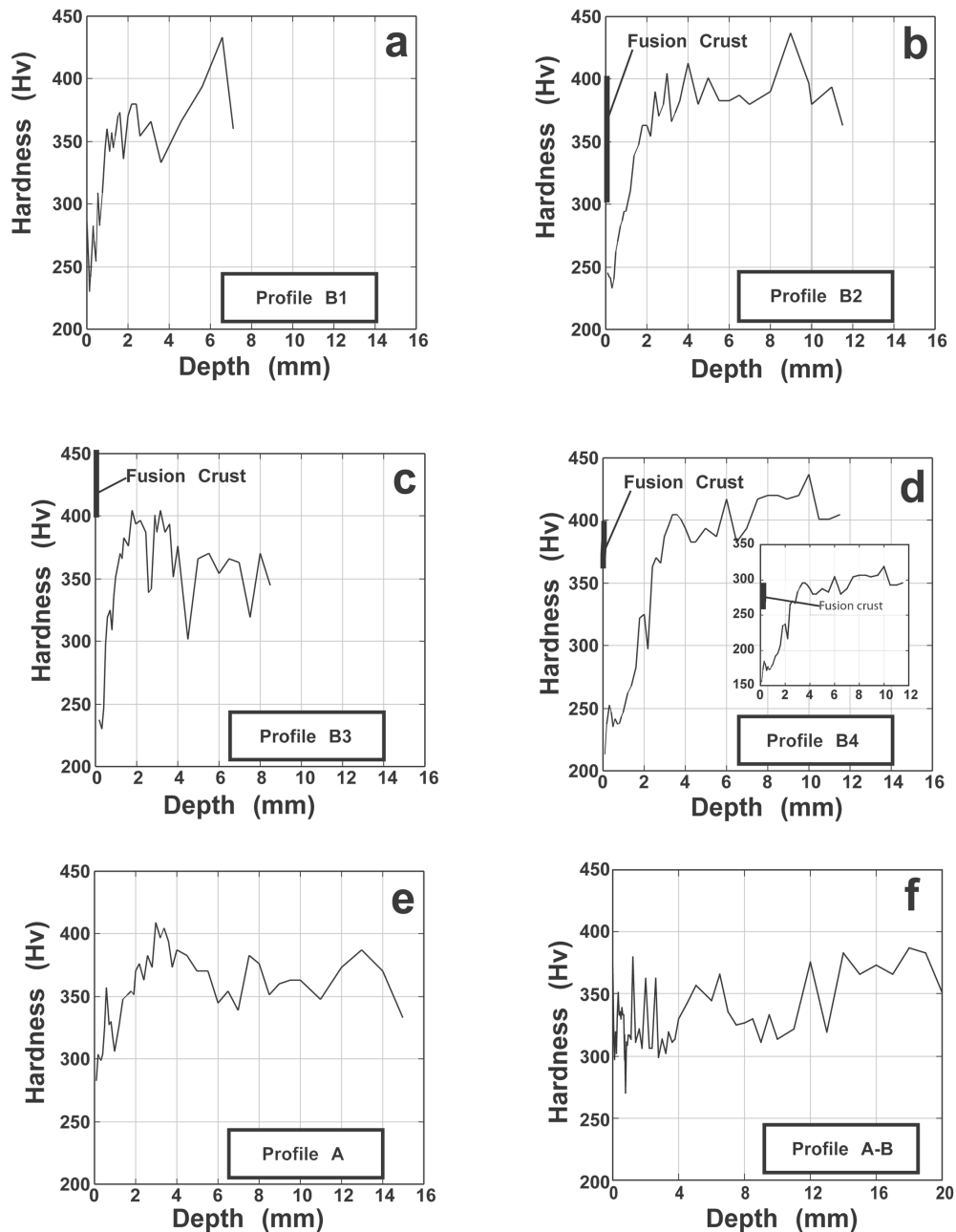


Fig. 4. Six hardness profiles (a–f) measured on three different meteorite surfaces. The location of the profiles is indicated in Fig. 1b. In (d) a correction of  $-27\%$  is applied on the raw hardness data, showing the hardness values shifted close to the range of shock-hardened octahedrite kamacite (Buchwald 1975).

- b. The second zone (recovery zone) of systematic hardness increase reaching its minimum depth of about 2 mm ( $HV\ 405 \pm 47$ ) in profile B3 (Fig. 4c) and a maximum depth of  $\sim 4$  mm ( $HV\ 413 \pm 47$ ) in profile B2 (Fig. 4b). This zone reaches a depth of about 2.6 mm (Fig. 4a) in profile B1 ( $HV\ 280 \pm 47$ ) and a depth of 3.5 mm (Fig. 4d) in profile B4 ( $HV\ 405 \pm 47$ ).
- c. The third zone in which the hardness remains more or less constant with increasing depth. This zone does not show heat-affect formed during atmospheric passage. It

is thought to resemble the unaltered interior of Shiṣr 043 with hardness values prior to atmospheric entry.

Hardness measurements obtained on surface A, profile A, lack the first zone as described above. Instead, the profile begins with the recovery zone but at a higher hardness with a minimum value  $HV\ 283 \pm 47$  (Fig. 4e). The zone extends to a depth of slightly less than 4 mm from which a sharp drop of hardness occurs before reaching the zone not affected by heat.

The hardness measured on profile A-B shows a distinctive behavior, different from other profiles (Fig. 4f). In

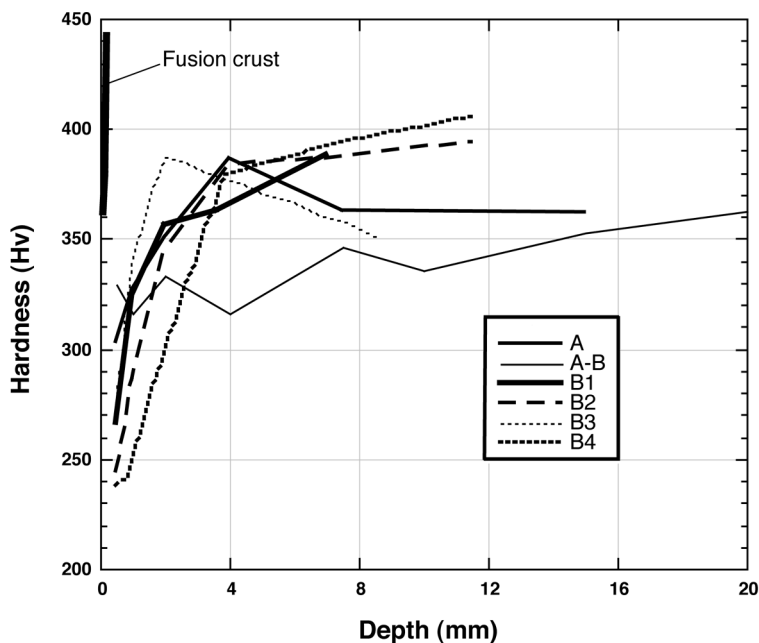


Fig. 5. Hardness averages for specific depth zones (0–0.5 mm, >0.5–1.0 mm, >1.0–2.0 mm, >2.0–4.0 mm, etc.) of the individual profiles, showing that the heat-affected zone probably extends to a depth of 7.1 mm in profile B1 (end of profile) and to a depth of 11.5 mm in profiles B2 and B4 (end of the profile). However, the heat-affected zone ends at 4 mm in profiles A, A-B, and B3.

the zone of 0–0.8 mm depth, the hardness varies from HV 270 to 376. In general this profile exhibits a wavy hardness profile from about 1 mm deep down to about 12 mm, followed by a jump of hardness down to 20 mm reaching a hardness of HV  $387 \pm 47$ .

The average Vickers hardness in the heat-unaffected interior of the meteorite is  $372 \pm 29$  ( $n = 95$ ) for kamacite and  $477 \pm 69$  ( $n = 29$ ) for taenite. The average estimated hardness error is  $HV \pm 47$  for all six profiles without the fusion crust. The average estimated hardness error for the metallic fusion crust is  $HV \pm 35$ .

Taking hardness averages for distinctive zones (0–0.5 mm, >0.5–1.0 mm, >1.0–2.0 mm, >2.0–4.0 mm, etc.), shows that the heat-affected zone probably extends to a depth of 7.1 mm (end of profile) in profile B1 and to a depth of 11.5 mm (end of the profile) in profiles B2 and B4 (Fig. 5).

Twelve hardness measurements obtained on a standard with known hardness, HV 585 at load of 100 g, gave a range between HV 592–689 and an average of  $HV 630 \pm 28$ , that is 7% higher than the standard. Thirteen hardness measurements made on the IA Odessa iron meteorite show a range of HV 228–279 and an average of  $HV 260 \pm 16$ , which is 29% higher than its typical value of HV 185 (Buchwald 1975). And 13 hardness measurements obtained on the IIB São Julião iron meteorite show a range of HV 230–264 and an average of  $HV 247 \pm 9$ , which is 24% higher than its typical value of HV 188 (Buchwald 1975).

Alteration products are found as thin crust of iron oxides and hydroxides (including magnetite, maghemite, and goethite) covering some parts of the surface of the meteorite,

and as fillings in impact-generated cracks penetrating to a depth of about 2 cm into the meteorite. By comparing the thickness of corrosion crust in sections from below the soil surface with sections from air-exposed parts of the meteorite, it is clear that corrosion is stronger in the buried parts, with a thickness of corrosion crust of 200–400  $\mu\text{m}$ , as compared with 50–80  $\mu\text{m}$  in the air-exposed part. The fusion crust also is better preserved in the exposed part. Taenite lamellae are significantly more resistant to weathering than kamacite.

### Chemistry of Fresh Metal

Chemical analyses of metal unaffected by weathering performed by several methods are summarized in Table 1. The average chemical composition of the fresh metal of Shişr 043 is very similar to the mean for IIIAB irons (Mittlefehldt et al. 1998) (Fig. 6 and Table 1). The values of Ir and As obtained by ICP-MS and of Ga obtained by INAA were not used for calculating the mean composition for Shişr 043 because these values are outside typical IIIAB ranges when considered together with Au (Wasson 1998). In case of ICP-MS, analytical uncertainties are clearly larger than for INAA data. The reason for the low value of Ga by INAA is unclear. The Ni content of Shişr 043 is in the range of the IIIAB, IIE, IIIE, and IVA groups. Analysis using the ICP-MS method show Cu, Ga, and Au contents very close to the Nyaung and Willison IIIAB meteorites (Wasson et al. 1998). A comparison of the chemical composition of Shişr 043 with other iron meteorites from the Arabian Peninsula shows that its chemical composition is very close to al-Ghanim (IIIAB)

Table 1. Chemical analyses of Shiṣr 043 compared to the mean of IIIAB irons.

Method		ICP-OES	AAS	ICP-MS	INAA	XRF	MEAN	Mean IIIAB <sup>a</sup>	Mean IIIAB <sup>b</sup>
Fe	wt%	91.60	90.5			90.9	91.00		
Co	wt%	0.50	0.53	0.52	0.45	0.49	0.50	0.49	0.50
Ni	wt%	8.08	8.1	8.08	8.10	7.97	8.07	8.6	8.49
P	wt%	0.14				0.12	0.13	0.19	0.56
Cr	ppm				78		78		40
Cu	ppm			174	125	134	144		160
Ga	ppm			18.80	14.4 <sup>c</sup>		18.80	18.80	19.70
Ge	ppm			36.20	38.3		37.25	37.30	38.90
As	ppm			8.5 <sup>c</sup>	3.3		5.9		10.5
Sb	ppm			0.06	0.06		0.06		0.265
W	ppm			1.40	1.34		1.37		1
Re	ppm			0.40	0.32		0.36		
Ir	ppm			1.8 <sup>c</sup>	3.92		3.92	0.014–20.7	4.1
Pt	ppm			14.30	6		10.15		
Au	ppm			0.60	0.58		0.59		1.2
Total	wt%						99.73		

<sup>a</sup>From Mittlefehldt et al. (1998).

<sup>b</sup>From Mason (1971).

<sup>c</sup>Values not used for calculation of average; see text.

ICP-OES = inductively coupled plasma optical emission spectrometry; AAS = atomic absorption spectrometry; ICP-MS = inductively coupled plasma mass spectrometry; INAA = instrumental neutron activation analysis; XRF = X-ray fluorescence analysis.

for most elements, and to Wabar (IIIAB) for Ga and Ge. But Wabar has a slightly lower concentration of Ni and a higher concentration of Ir (Grady 2000). Relations between Au and a range of elements (Ga, Ge, Sb, Co, As, Ni, Cu, W, Ir) show that Shiṣr 043 occupies a position within the IIIAB population as shown by Wasson et al. (1998).

### Chemistry of Weathering Products and Soil

The part of the meteorite originally buried in the soil is partially covered by reddish brown, strongly magnetic flakes of iron (hydr)oxides resulting from weathering of the iron meteorite. Five types of materials reflecting different interactions between meteorite and soil were analyzed and compared with unaltered meteorite and reference soil (Table 2). Two types of weathered flakes were distinguished: coarse (3–20 mm) flakes directly attached to the meteorite (Table 2, column 1) and fine flakes (0.5–2 mm) found next to the coarse flakes and on the soil below the meteorite (Table 2, column 2). Coarse flakes were hand-picked, fine flakes were separated as highly magnetic separate from the 0.15–2 mm soil fraction. Soil (<0.15 mm) adhering to meteoritic material was separated into a magnetic (Table 2, column 3) and a nonmagnetic fraction (Table 2, column 4). A sample of soil from beneath the meteorite (Table 2, columns 5 and 6, SUM) representing material in less direct contact with the meteorite than adhering soil and a reference soil sample (Table 2, columns 7 and 8, RSS) were also analyzed by bulk- and aqua regia leach methods (fraction <0.15 mm in both cases).

Chemical analyses of major oxides show that meteoritic elements in the coarse flakes are diluted due to the addition of O and H. Concentrations of meteoritic elements (Fe, Ni, Co,

P, Cu, Ge, and Ir) decrease in the order: coarse oxide, fine oxide, adhering soil (magnetic and nonmagnetic), SUM, and RSS. In the same sequence, typical soil elements (CaO, Al<sub>2</sub>O<sub>3</sub>) and most trace elements increase due to increasing soil components. The adhering soil (magnetic and nonmagnetic) is enriched in elements typically concentrated in heavy minerals such as V, Cr, Zn, and Zr, possibly due to a wind-induced heavy mineral enrichment. Still, Ni and Co occur in meteoritic proportions in the magnetic fraction. In the nonmagnetic fraction, Ni/Co is increased relative to the magnetic fraction indicating a preferential transfer of relatively mobile Ni from the oxide fraction to nonmagnetic soil particles. Sr/Ca ratios are much higher in the meteorite oxide than in the soil, proving a preferential enrichment of Sr during weathering as is commonly observed in chondrites (Al-Kathiri et al. 2005). Barium, on the other hand, is not strongly enriched as in chondrites but bound to soil material. Other elements enriched in the oxides are Mo (based on bulk concentrations) and U (based on Th/U ratios of 3.4–4.4 in soils and 1.7–1.9 in fine oxides).

Comparing the chemical composition of the coarse and fine oxide flakes with the mean composition of medium octahedrites (Om) and/or IIIAB (Mason 1971) shows that the oxide flakes are clearly depleted in the major elements commonly related to iron meteorites such as Fe, Co, Ni, Ga, and Ge (Fig. 6 and Table 2), with a possible loss of Fe, Ni, and Co relative to Ga and Ge in the fine fraction. However, the magnetic fraction of the adherent soil is enriched in Ga relative to the oxide flakes (Fig. 6).

In both leached soil analyses and total soil analyses (Table 2) the concentrations of Ni and Co and the ratios of Ni/Fe and Ni/Co are higher in the SUM sample than in the RSS,

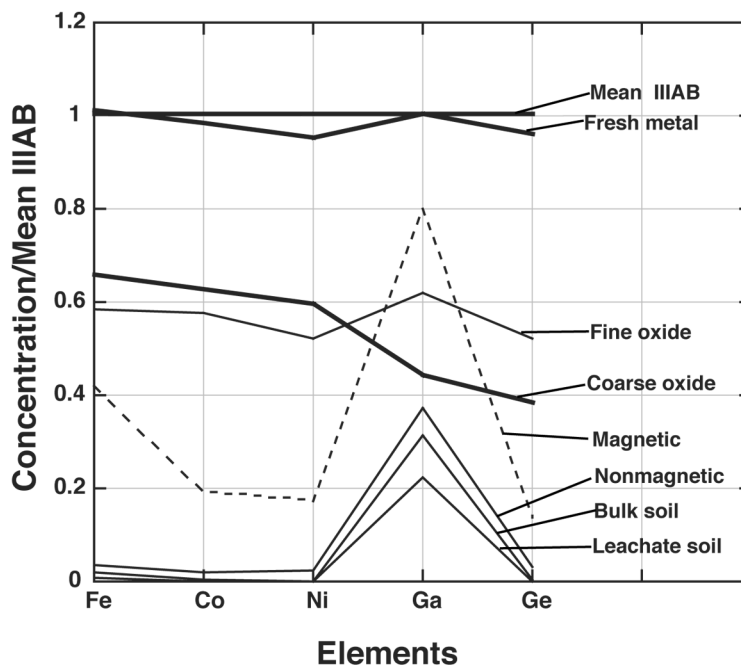


Fig. 6. Fe, Co, Ni, Ga, and Ge contents normalized to the mean composition of IIIAB irons (Mittlefehldt et al. [1998] and Mason [1971]). Shişr 043 metal is very similar to mean IIIAB iron meteorites. Both coarse and fine oxide flakes show dilution of meteoritic components. The magnetic and nonmagnetic fraction from adherent soil and the soil under meteorite show a systematic decrease in the major elements commonly related to iron meteorites. Ga in fine oxides indicates contamination from soil.

indicating a transfer of Ni and Co from the meteorite to the soil. The total bulk soil analysis shows a high Cr concentration in both the SUM (865 ppm) and the RSS sample (1550 ppm) compared to the mean upper crustal value of 35 ppm (Taylor and McLennan 1985), a feature commonly observed in Oman desert soils (Al-Kathiri et al. 2005).

### Cosmogenic Noble Gases

For the partitioning of the noble gases into the cosmogenic (*c*), trapped (*tr*), and radiogenic (*r*) components, certain assumptions have to be made: solar noble gases have never been observed in iron meteorites. Thus, we assume that no trapped solar He, Ne, and Ar are present in our sample. This assumption is supported by the observed  $^{36}\text{Ar}/^{38}\text{Ar}$  ratio of  $0.652 \pm 0.007$  that is close to the purely cosmogenic value of  $\sim 0.65$  for small iron meteorites (Lavielle et al. 1999). Radiogenic  $^4\text{He}$  is also assumed to be negligibly small relative to cosmogenic  $^4\text{He}$ : we observe a  $^4\text{He}/^3\text{He}$  ratio of  $3.1 \pm 0.04$ , a ratio that is usually observed for the cosmogenic component of surface samples of iron meteorites (Fechtig et al. 1960; Signer and Nier 1960; Voshage 1982; Voshage and Feldmann 1979; Voshage et al. 1983). Furthermore, as  $(^{40}\text{Ar}/^{38}\text{Ar})_c = 0.2$  (Eugster et al. 1993),  $^{40}\text{Ar}$  is essentially of radiogenic origin from  $^{40}\text{K}$  decay. Data for noble gases are given in Tables 3 and 4.

Most isotopic ratios of the cosmic-ray produced noble gases depend on the meteoroid size and the shielding depth of

the investigated sample within the meteoroid. For observed trends and the information on this subject see the references given above. Depth-sensitive cosmogenic noble gas ratios include  $^4\text{He}/^3\text{He}$ ,  $^4\text{He}/^{21}\text{Ne}$ , and  $^4\text{He}/^{38}\text{Ar}$ , whereas the  $^3\text{He}/^{38}\text{Ar}$  is relatively constant at 16–17. In lightly shielded iron meteorite samples the  $^4\text{He}/^3\text{He}$  ratio is about 3, and the  $^4\text{He}/^{21}\text{Ne}$  and  $^4\text{He}/^{38}\text{Ar}$  ratios are in the range of 190–250 and 50–60, respectively. The cosmogenic noble gas ratios obtained from Shişr 043 (Table 4) are in the range of the values given above.

The production rates of cosmogenic noble gases and radionuclides in iron meteorites are strongly dependent on shielding conditions. The  $^4\text{He}/^{21}\text{Ne}$  ratio of  $229 \pm 9$  in Shişr 043 is similar to  $^4\text{He}/^{21}\text{Ne}$  ratios of 227–237 found in four small iron meteorites (Brownfield, Carlton, Morradal, Norfolk) studied by Lavielle et al. (1999). We used the published noble gas data and the  $^{10}\text{Be}$ - $^{21}\text{Ne}$  and  $^{36}\text{Cl}$ - $^{36}\text{Ar}$  ages of these four meteorites to determine the average production rates of  $^3\text{He}$ ,  $^{21}\text{Ne}$  and  $^{38}\text{Ar}$  in small irons. We thus derived a  $^3\text{He}$  production rate ( $P_3$ ) of  $132 \pm 10$ , a  $^{21}\text{Ne}$  production rate ( $P_{21}$ ) of  $1.96 \pm 0.08$ , and a  $^{38}\text{Ar}$  production rate ( $P_{38}$ ) of  $8.15 \pm 0.44$ , all in units of  $10^{-10} \text{ cm}^3 \text{ STP/g per Ma}$ . The resulting CRE ages,  $T_i$ , are obtained from  $T_i = N_i/P_i$ , where  $i$  is the mass and  $N$  the concentration of the cosmogenic nuclide. From the measured  $^3\text{He}$ ,  $^{21}\text{Ne}$ , and  $^{38}\text{Ar}$  concentrations, we thus calculate ages of  $309 \pm 26 \text{ Ma}$ ,  $281 \pm 17 \text{ Ma}$ , and  $316 \pm 20 \text{ Ma}$ , respectively, yielding a (weighted) average age of  $298 \pm 12 \text{ Ma}$ .

Table 2. Analyses of Shiřr 043 weathering products and soil.

Units		Oxide flakes		Adhering soil		SUM		RSS	
		Coarse	Fine	Magnetic	Non-magnetic	Bulk	Leachate	Bulk	Leachate
		1	2	3	4	5	6	7	8
SiO <sub>2</sub>	%	1.28	3.19	15.74	47.64				
Al <sub>2</sub> O <sub>3</sub>	%	0.16	0.43	3.95	6.13	4.48	0.91	4.47	0.82
Fe <sub>2</sub> O <sub>3</sub>	%	84.94	75.82	54.42	4.74	2.40	1.19	2.96	1.14
MnO	%	<0.01	0.01	0.27	0.08	0.06	0.03	0.07	0.02
MgO	%	0.16	0.35	3.45	2.79	2.62	1.49	2.40	1.29
CaO	%	0.84	1.81	4.16	17.43	19.62	21.65	19.97	20.44
Na <sub>2</sub> O	%	0.24	0.25	0.84	1.50	1.31	0.06	1.13	0.04
K <sub>2</sub> O	%	0.11	<0.01	0.41	1.18	1.31	0.09	1.27	0.08
TiO <sub>2</sub>	%	0.02	0.16	6.20	1.30	0.67	0.09	1.06	0.10
P <sub>2</sub> O <sub>5</sub>	%	0.22	0.17	0.07	0.06	0.03	0.03	0.03	0.02
LOI	%	8.44	10.91	7.52	15.88				
Total	%	96.41	93.10	97.02	98.74				
Sc	ppm	2	2	16	10	7	2.3	8	2.2
V	ppm	<5	35	824	80	51	24	65	25
Cr	ppm	75	243	7310	1490	865	26	1550	26
Fe	%	59.4	53.0	38.1	3.3	1.68	0.83	2.07	0.80
Co	ppm	3119	2892	957	103	12.1	8	9.5	4
Ni	ppm	50,150	44,400	14,500	2025	125	110	50.2	29
Cu	ppm	59	69	44	20	8.4	9	8.1	10
Zn	ppm	<30	<30	314	42	24	26	31	28
Ga	ppm	8	12	15	7	5.9	4	5.8	4
Ge	ppm	15	20	5.3	1.2	0.2		0.3	
Rb	ppm	<2	2	11	30	25.8		24.3	
Sr	ppm	191	580	301	376	296	241	272	202
Y	ppm	<1	1.3	10.3	18.6	11.0	5	13.6	5
Zr	ppm	16	33	209	730	124	7	172	7
Nb	ppm	<1	<1	27	15	8.2		9.7	
Mo	ppm	24	19	20	17	2	<0.5	1	<0.5
Ba	ppm	7	34	111	240	252	48	241	35
La	ppm	0.1	1.3	9.3	17.2	15.6	6	22.0	5
Ce	ppm	0.3	2.3	21.1	32.2	29.8		43.7	
Pr	ppm	<0.05	0.2	1.7	3.2	3.8		5.3	
Nd	ppm	0.1	1.0	8.0	13.7	14.7		20.9	
Sm	ppm	<0.1	0.2	1.9	3.2	2.9		4.2	
Eu	ppm	<0.05	<0.1	0.5	0.7	0.66		0.81	
Gd	ppm	<0.1	0.2	1.8	3.0	2.7		3.7	
Tb	ppm	<0.1	<0.1	0.3	0.5	0.4		0.5	
Dy	ppm	<0.1	0.2	1.8	3.1	2.3		3.1	
Ho	ppm	<0.1	<0.1	0.4	0.6	0.5		0.7	
Er	ppm	<0.1	0.1	1.2	2.2	1.5		1.8	
Tm	ppm	<0.1	<0.1	0.2	0.4	0.2		0.3	
Yb	ppm	<0.1	0.1	1.2	2.2	1.4		1.9	
Lu	ppm	<0.1	<0.1	0.2	0.4	0.2		0.3	
Hf	ppm	0.3	0.7	5.0	17.2	3.0		4.3	
Ta	ppm	<0.1	<0.1	2.2	1.1	0.5		0.3	
Th	ppm	<0.1	0.6	2.9	6.4	5.0		8.4	
U	ppm	<0.1	0.3	1.5	2.0	1.5		1.9	
Ni/Fe		0.084	0.084	0.038	0.061	0.007	0.013	0.002	0.004
Ni/Co		16.08	15.35	15.15	19.66	10.36	13.38	5.30	8.05
Sr/Ca		0.032	0.045	0.010	0.003	0.002	0.002	0.002	0.001
Th/U			1.71	1.94	3.20	3.44		4.40	

Be <1, W <1, In <0.2, Ag <0.5, Tl <0.1 [ppm]

Analytical method: ICP-MS except for Fe (ICP-OES)

LOI = loss of ignition

1 = strongly magnetic oxide flakes, several mm to 2 cm in size; 2 = strongly magnetic fine oxide flakes, fraction 0.5–2 mm; 3 = soil material originally adhering to coarse oxide flakes, sieved to <0.15 mm, magnetic fraction; 4 = soil material originally adhering to coarse oxide flakes, sieved to <0.15 mm, nonmagnetic fraction; 5 = soil collected under the meteorite, bulk analysis; 6 = soil collected under the meteorite, aqua regia leach analysis of fraction <0.15 mm; 7 = reference soil collected 10 m from meteorite, fraction <0.15 mm, bulk analysis; 8 = reference soil collected 10 m from the meteorite, fraction <0.15 mm, aqua regia leach analysis

Table 3. Noble gas isotope data for a 52.45 mg split of Shişr 043 (concentrations in  $10^{-8}$  cm<sup>3</sup> STP/g).

<sup>4</sup> He	<sup>20</sup> Ne	<sup>40</sup> Ar	<sup>4</sup> He/ <sup>3</sup> He	<sup>20</sup> Ne/ <sup>22</sup> Ne	<sup>22</sup> Ne/ <sup>21</sup> Ne	<sup>36</sup> Ar/ <sup>38</sup> Ar	<sup>40</sup> Ar/ <sup>36</sup> Ar
1260 ± 40	5.66 ± 0.20	35.1 ± 1.8	3.11 ± 0.04	0.929 ± 0.02	1.106 ± 0.02	0.652 ± 0.007	2.08 ± 0.09

Table 4. Cosmogenic noble gases (concentrations in  $10^{-8}$  cm<sup>3</sup> STP/g, age in Ma).

<sup>3</sup> He	<sup>21</sup> Ne	<sup>38</sup> Ar	<sup>4</sup> He/ <sup>3</sup> He	<sup>4</sup> He/ <sup>21</sup> Ne	<sup>4</sup> He/ <sup>38</sup> Ar	<sup>22</sup> Ne/ <sup>21</sup> Ne	CRE age
406 ± 14	5.50 ± 0.25	25.8 ± 0.9	3.11 ± 0.05	229 ± 9	50 ± 3.0	1.09 ± 0.02	298 ± 12

Assumptions: <sup>3</sup>He<sub>ir</sub> = 0, <sup>4</sup>He<sub>ir</sub> = 0, (<sup>20</sup>Ne/<sup>22</sup>Ne)<sub>c</sub> = 0.8, (<sup>20</sup>Ne/<sup>22</sup>Ne)<sub>ir</sub> = 9.8, (<sup>21</sup>Ne/<sup>22</sup>Ne)<sub>ir</sub> = 0.029, (<sup>36</sup>Ar/<sup>38</sup>Ar)<sub>c</sub> = 0.64, (<sup>36</sup>Ar/<sup>38</sup>Ar)<sub>ir</sub> = 5.32.

Table 5. Concentrations of cosmogenic radionuclides (in dpm/kg) in Shişr 043.

Mass (mg)	<sup>10</sup> Be	<sup>26</sup> Al	<sup>36</sup> Cl	<sup>41</sup> Ca
97.8	5.62 ± 0.11	3.94 ± 0.12	24 ± 1	28 ± 2

### Cosmogenic Radionuclides

We also used the measured concentrations of <sup>10</sup>Be, <sup>26</sup>Al, and <sup>36</sup>Cl (Table 5) as internal shielding parameters for calculating the production rates of <sup>21</sup>Ne and <sup>36</sup>Ar. Based on the <sup>10</sup>Be-<sup>21</sup>Ne, <sup>26</sup>Al-<sup>21</sup>Ne, and <sup>36</sup>Cl-<sup>36</sup>Ar methods (Lavielle et al. 1999), we find CRE ages of 275 ± 14 Ma (<sup>10</sup>Be-<sup>21</sup>Ne), 271 ± 15 Ma (<sup>26</sup>Al-<sup>21</sup>Ne), and 299 ± 15 Ma (<sup>36</sup>Cl-<sup>36</sup>Ar) for Shişr 043. These three ages yield an average CRE age of 282 ± 12 Ma, consistent with the age calculated above. Finally, the high <sup>41</sup>Ca concentration of 28 ± 2 dpm/kg is indistinguishable from the saturation value of 24 ± 2 dpm/kg (Fink et al. 1991), indicating a very short terrestrial age.

## DISCUSSION

### The Shişr 043 Iron Meteorite Find

It is unclear why the fraction of iron meteorites among all finds in Oman is as low as 0.07%. With more than 1400 meteorites reported from Oman and irons constituting 5% of observed meteorite falls (Grady 2000; McSween 1999; Norton 2002), about 60 iron meteorites should have been found in Oman. There are two possible explanations for this anomaly: a) due to the easy recognition of the iron meteorites they may have been collected by ancient inhabitants or people passing through the Oman desert across the old trade routes; b) due to the high density of the iron meteorites (~8 gcm<sup>-3</sup>), they are more likely to slowly sink into the sandy soil and finally be completely covered. The first possibility is not supported by finds of tools made of meteoritic iron in Oman or nearby countries, as it is the case for ancient Egypt (Bevan and Laeter 2002). The second possibility is supported by the fact that many meteorites found during our search program were almost submerged in the soil. Also, heavy steel drill bits from oil exploration (within less than 50 years) were found buried by 50–80% in the soil. The second possibility may also explain the relatively high abundance of lunar and Martian meteorites in Oman, as they are less dense compared to chondrites and iron meteorites so their tendency to sink in the

soil is less pronounced. Shişr 043 was found on a subrecent alluvial fan. Possibly it was partly reexposed to the surface as a result of reworking of the alluvial fan during rare flood periods.

### Structure, Mineralogy, and Microhardness

The average kamacite bandwidth of 1.0 ± 0.1 mm leads to a structural classification as medium octahedrite (Om). Medium octahedrites are represented in the groups IIIAB and IAB but not in the chemically similar groups IIE (Ogg) and IIIE (Og). The structure of Shişr 043 is fully consistent with a IIIAB classification. The generally high hardness indicates that the meteorite has been strongly shocked during its pre-atmospheric history, probably as part of its parent body history. The high shock record is supported by the fine-grained heat-affected zone  $\alpha_2$  (Buchwald 1975) and the observation of Neumann lines on a well-etched slab (Norton 2002). The strongly shocked nature also is characteristic for the IIIAB group (Buchwald 1975). The metallic fusion crust and the heat-affected zone of Shişr 043 have deviating hardness values. The hardness measured on the steel standard, the IA Odessa, and the IIB iron São Julião de Moreira is higher than their typical hardness values as reported by Buchwald (1975). Even the measured minimum values are higher than their typical hardness values indicating an instrumental error tending towards high hardness. The smaller error for the standard steel (7%) but larger error for the iron meteorites (24–29%, average 27%) is probably caused by their larger compositional and/or structural variation. By applying a correction of -27% on the hardness obtained from profile B4 made on surface B the hardness values are shifted close to the range of kamacite (Fig. 4d) from typical octahedrite (Buchwald 1975).

Hardness profiles on surfaces A, B, and at the intersection between the two surfaces show different behaviors for each surface indicating different heat-effects during the meteorite's atmospheric travel. In general, measurable heating effects corresponding to a heating exceeding 750 °C (Buchwald 1975) reach to a depth of

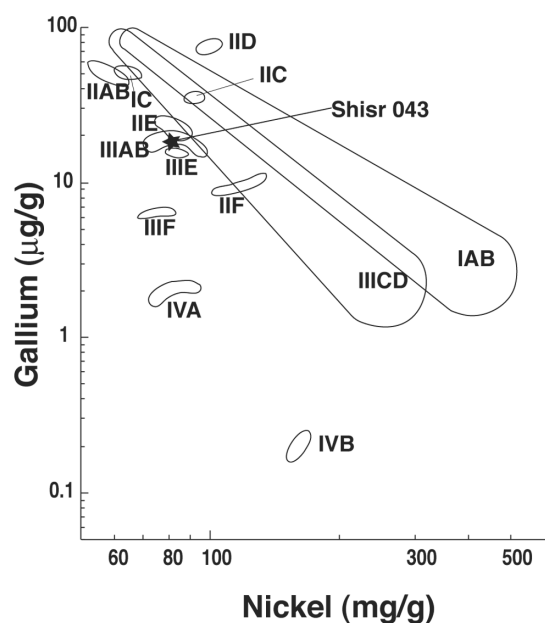


Fig. 7. A plot of Ni versus Ga clearly positions the meteorite in the field of IIIAB group.

1.2 mm and heating to 300–750 °C reach to a depth of 4 mm, corresponding to the hardness-affected recovered zone of (Buchwald 1975).

### Chemistry of Fresh Metal

The fresh metal chemical composition is in the range of the IIIAB group (Mason 1971, Wasson 1998, Mittlefehlt et al. 1998) and there are no indications that Shiṣr 043 does not fit into this group. Its Cu, Ga, and Au contents are very close to those of the meteorites Nyaung and Willison IIIAB and its average composition is close to the al-Ghanim medium octahedrite (Wasson et al. 1998). The Ni content is in the range of IIIAB, IIE, IIIE, IAB, and IVA groups. The IIE and IIIE are the nearest chemical groups to the IIIAB group, but in this case they can be excluded due to their high Cu content, lower Ga content in IIIE group, and slightly higher Ga content in IIE group (Mittlefehlt et al. 1998). In a Ga versus Ni plot, Shiṣr 043 falls in the field of IIIAB group (Fig. 7). Groups IAB and IVA are clearly excluded due to their different contents of Ga (Fig. 7) and P. Based on the work of Wasson (1999) and contents of Ir, Au, and As, Shiṣr 043 represents a sample of the IIIAB core formed after ~35% solidification and not including significant amounts of trapped melt. The latter conclusion is also in agreement with the very low sulfur content of Shiṣr 043.

### Comparison with Other Iron Meteorites from the Arabian Peninsula

Besides Shiṣr 043, eight iron meteorites are known from the Arabian Peninsula (Table 6), all from Saudi Arabia (Holm

1962). Although these finds were made 141 to >900 km from Shiṣr 043, we will consider them for possible pairing (Table 6) as there is evidence for human transport of Wabar masses (Grady 2000). The al-Ghanim (IIIAB) iron meteorite is closest to Shiṣr 043 in terms of distance, structural classification, and, except for small variations, chemical composition. However, al-Ghanim is strongly oxidized whereas Shiṣr 043 shows only minor oxidation on the surface of the part submerged in soil and in thin fractures <2 cm deep; thus they likely have very different terrestrial ages. Wabar is similar in its chemical (IIIAB) and structural classification (Om), but differs by its lower Ni content (7.62 wt%) and higher Ir content (6 ppm). Also, Wabar is medium-shocked as revealed by microhardness (Buchwald 1975), in contrast to the strongly shocked Shiṣr 043. The small pre-atmospheric mass indicated by cosmogenic noble gas ratios and radionuclide concentrations also is an argument against pairing of Shiṣr 043 with the large Wabar meteorite. Naif is reported to be a transported piece of Wabar, whereas South Dhana and ar-Rakhbah are strongly oxidized. Alkhamasin is excluded because of its different structural (Ogg) and chemical classification (IIAB). No data are available for the small and distant Rub' al-Khali 003 iron.

### Chemistry of Altered Metal and Soil

The iron oxide flakes are weathered parts from the iron meteorite as is confirmed by their high contents of P, Ni, Co, Ge, Ir. The flakes are restricted to the part of the meteorite buried in the soil. The surface of the buried part is more strongly weathered because it is more subjected to moisture captured by the soil from night dew, slower water evaporation after rare rain showers, and salts concentrated in the soil. Besides mechanical soil admixtures, meteoritic iron oxide can be shown to have accumulated Sr, Mo, and U from the soil. Sr accumulation is also common in chondrites. Due to the low concentration of sulfur in Shiṣr 043 (as troilite), Sr capturing due to release of sulfate resulting from sulfide oxidation and precipitation of SrSO<sub>4</sub> appears unlikely here. The higher Co and Ni content in the SUM sample compared to the RSS sample clearly indicate contamination from the meteorite to the underlying soil as observed under many chondrites (Al-Kathiri et al. 2005).

### Pre-Atmospheric Size, and CRE- and Terrestrial Ages

Considering the uncertainties in the measured <sup>41</sup>Ca concentration as well as in the saturation value, we can only constrain the terrestrial age to less than 10 kyr. Based on the radionuclide concentrations alone we cannot exclude the possibility that Shiṣr 043 is a recent fall, although an age of at least several decades seems likely considering the significant amount of weathering products found on the buried part of the meteorite.

The average CRE age calculated from cosmogenic <sup>3</sup>He,



$^{21}\text{Ne}$ , and  $^{38}\text{Ar}$  and the corresponding production rates given above is  $298 \pm 12$  Ma. This age is consistent with the average CRE age of  $282 \pm 12$  Ma based on the  $^{10}\text{Be}$ - $^{21}\text{Ne}$ ,  $^{26}\text{Al}$ - $^{21}\text{Ne}$ , and  $^{36}\text{Cl}$ - $^{36}\text{Ar}$  methods. We therefore adopted a mean value of  $290 \pm 20$  Ma ( $2\sigma$ ) as the preferred CRE age. This age falls within the range of ages found for IIIAB irons, but does not coincide with the cluster around 650 Ma observed in the  $^{40}\text{K}$ - $^{41}\text{K}$  exposure age distribution (Wieler 2002) or with the corresponding cluster around  $\sim 450$  Ma in the  $^{36}\text{Cl}$ - $^{36}\text{Ar}$  distribution (Lavielle et al. 1999).

The cosmogenic noble gases (Table 4) indicate that the sample that we analyzed originates from the surface layer of the meteoroid or that the pre-atmospheric size of the meteoroid was relatively small. The high  $^{10}\text{Be}$  and  $^{26}\text{Al}$  concentrations indicate that Shiřr 043 had a pre-atmospheric radius between 10 and 25 cm. If we consider that this meteorite had a small pre-atmospheric mass, this will make it unlikely to be paired with any of the iron meteorite finds from the Arabian Peninsula.

### CONCLUSIONS

Shiřr 043 is a single, 8267 g mass of a type IIIAB iron meteorite showing preserved metallic fusion crust and heat-affected zones. The kamacite bandwidth, the chemical composition, and the Vickers hardness (HV) all are consistent with a strongly shocked IIIAB medium octahedrite classification for Shiřr 043. The accumulation of fusion crust on the concave surface B, the variable thicknesses of the heat-affected zone at surface A and surface B, and the variable hardness profiles from different surface types indicate that each surface was subjected to different heating conditions during atmospheric trajectory. Cosmogenic isotope ratios indicate that Shiřr 043 had a small pre-atmospheric mass, its CRE age of  $290 \pm 20$  Ma is characteristic for the IIIAB group iron age range, and the  $^{41}\text{Ca}$  saturation points to a subrecent fall. Also, young terrestrial age is supported by the presence of metallic fusion crust and heat-affected zones indicating minor removal of material from the meteorite as a result of weathering. Shiřr 043 is the only iron meteorite so far reported from Oman, while many more should be expected among  $>1400$  Oman meteorite finds, based on a 5% proportion among observed falls. This anomaly may be due to collecting or preferential sinking of heavy irons into the soil. Shiřr 043 seems not to be paired with any of the other iron meteorite finds from the Arabian Peninsula.

*Acknowledgments*—Dr. Hilal Al Azri, Ministry of Commerce and Industry, Muscat; Akram Al Muraza, Khalid Musallam Al Rawas; and Sami Al Zubaidi, Ministry of Commerce and Industry, Salalah, are thanked for their support during the project. Manuel Eggimann performed the XRF measurements and Peter Marmet helped with cutting and etching of the

meteorite. We thank Henning Haack for constructive comments on the manuscript. This study was supported by the Swiss National Science Foundation (grants 2100-064929 and 200020-107681).

*Editorial Handling*—Dr. Hiroko Nagahara

### REFERENCES

- Al-Kathiri A., Hofmann B. A., Jull A. J. T., and Gnos E. 2005. Weathering of meteorites from Oman: Correlation of chemical and mineralogical weathering proxies with  $^{14}\text{C}$  terrestrial ages and the influence of soil chemistry. *Meteoritics & Planetary Science* 40:1215–1239.
- Albrecht A., Schnabel C., Vogt S., Xue S., Herzog G. F., Begemann F., Weber H. W., Middleton R., Fink D., and Klein J. 2000. Light noble gases and cosmogenic radionuclides in Estherville, Budulan, and other mesosiderites: Implications for exposure histories and production rates. *Meteoritics & Planetary Science* 35:975–986.
- Aylmer D., Bonanno V., Herzog G. F., Weber H., Klein J., and Middleton R. 1988.  $^{26}\text{Al}$  and  $^{10}\text{Be}$  production rates in iron meteorites. *Earth and Planetary Science Letters* 88:107–118.
- Bevan A. and Laeter D. 2002. *Meteorites: A journey through space and time*. Washington, D. C: Smithsonian Books. 256 p.
- Bevan A. W. R., Bland P. A., and Jull A. J. T. 1998. Meteorite flux in the Nullarbor region, Australia. In *Meteorites: Flux with time and impact effects*, edited by Grady M. M., Hutchinson R., McCall G. J. H., and Rothery D. A. London: The Geological Society. pp. 59–73.
- Buchwald V. F. 1975. *Handbook of iron meteorites: Their history, distribution, composition, and structure*. Los Angeles: University of California Press. 1375 p.
- Chevrel S., Berthiaux A., Platel J. P., and Roger J. 1992. Explanatory notes to Geological map of Shiřr, sheet NF 39-08, scale 1: 250,000. Muscat: Sultanate of Oman, Ministry of Petroleum and Minerals.
- Eugster O., Michel T., Niedermann S., Wang D., and Yi W. 1993. The record of cosmogenic, radiogenic, fissionogenic, and trapped noble gases in recently recovered Chinese and other chondrites. *Geochimica et Cosmochimica Acta* 57:1115–1142.
- Fechtig H., Gentner W., and Kristen G. 1960. Räumliche Verteilung der Edelgasisotope im Eisenmeteoriten Treysa. *Geochimica et Cosmochimica Acta* 18:72–80.
- Fink D., Klein J., Middleton R., Vogt S., and Herzog G. F. 1991.  $^{41}\text{Ca}$  in iron falls, Grant and Estherville: Production rates and related exposure age calculations. *Earth and Planetary Science Letters* 107:115–128.
- Grady M. M. 2000. *Catalogue of meteorites*. 5th ed. Cambridge: Cambridge University Press. 696 p.
- Grossman J. N. 2000. The Meteoritical Bulletin, No. 84. *Meteoritics & Planetary Science* 35:A199–A225.
- Grossman J. N. and Zipfel J. 2001. The Meteoritical Bulletin, No. 85. *Meteoritics & Planetary Science* 36:A293–A322.
- Holm D. A. 1962. New meteorite localities in the Rub' Al Khali, Saudi Arabia. *American Journal of Science* 260:303–309.
- Lavielle B., Marti K., and Caffee M. W. 1999. The  $^{36}\text{Cl}$ - $^{36}\text{Ar}$ - $^{40}\text{K}$ - $^{41}\text{K}$  records and cosmic ray production rates in iron meteorites. *Earth and Planetary Science Letters* 170:93–104.
- Mason B. 1971. *Handbook of elemental abundance in meteorites*. New York: Gordon & Breach. 555 p.
- McSween H. Y., Jr. 1999. *Meteorites and their parent planets*. Cambridge: Cambridge University Press. 310 p.

- Mittlefehldt D. W., McCoy J. T., Goodrich C. A., and Kracher A. 1998. Non-chondritic meteorites from asteroidal bodies. In *Planetary materials*, edited by Papike J. J. Washington, D. C.: The Mineralogical Society of America. pp. 1–195.
- Nishiizumi K. 2004. Preparation of  $^{26}\text{Al}$  AMS standards. *Nuclear Instruments and Methods in Physics Research B* 223–224:388–392.
- Nishiizumi K., Caffee M. W., and DePaolo D. J. 2000. Preparation of  $^{41}\text{Ca}$  AMS standards. *Nuclear Instruments and Methods in Physics Research B* 172:399–403.
- Nishiizumi K., Elmore D., Ma X. Z., and Arnold J. R. 1984.  $^{10}\text{Be}$  and  $^{26}\text{Al}$  depth profiles in an Apollo 15 drill core. *Earth and Planetary Science Letters* 70:157–163.
- Norton O. R. 2002. *The Cambridge encyclopedia of meteorites*. Cambridge: Cambridge University Press. 354 p.
- Roberts M. L., Bench G. S., Brown T. A., Caffee M. W., Finkel R. C., Freeman S. P. H. T., Hainsworth L. J., Kashgarian, McAninch J. E., Proctor I. D., Southon J. R., and Vogel J. S. 1997. The LLNL AMS facility. *Nuclear Instruments and Methods in Physics Research B* 123:57–61.
- Russell S. S., Zolensky M. E., Righter K., Folco L., Jones R., Connolly H. C., Grady M. M., and Grossman J. N. 2005. The Meteoritical Bulletin, No. 89. *Meteoritics & Planetary Science* 40:A201–A263.
- Russell S. S., Folco L., Grady M. M., Zolensky M. E., Jones R., Righter K., Zipfel J., and Grossman J. N. 2004. The Meteoritical Bulletin, No. 88. *Meteoritics & Planetary Science* 39:A215–A272.
- Russell S. S., Zipfel J., Folco L., Jones R., Grady M. M., Zolensky M. E., McCoy T., and Grossman J. N. 2003. The Meteoritical Bulletin, No. 87. *Meteoritics & Planetary Science* 38:A189–A248.
- Russell S. S., Zipfel J., Grossman J. N., and Grady M. M. 2002. The Meteoritical Bulletin, No. 86. *Meteoritics & Planetary Science* 37:A157–A184.
- Schlüter J., Schultz L., Thiedig B., Al-Mahdi B. O., and Abu Aghreb A. E. 2002. The Dar al Gani meteorite field (Libyan Sahara): Geological setting, pairing of meteorites, and recovery density. *Meteoritics & Planetary Science* 37:1079–1093.
- Sharma P., Kubik P. W., Fehn U., Gove G. E., Nishiizumi K., and Elmore D. 1990. Development of  $^{36}\text{Cl}$  standards for AMS. *Nuclear Instruments and Methods B* 52:410–415.
- Signer P. and Nier A. O. 1960. The distribution of cosmic-ray-produced rare gases in iron meteorites. *Journal of Geophysical Research* 65:2947–2964.
- Taylor S. R. and McLennan S. M. 1985. *The continental crust: Its composition and evolution*. Oxford: Blackwell Scientific Publications. 312 p.
- Voshage H., Feldmann H., and Braun O. 1983. Investigations of cosmic-ray-produced nuclides in iron meteorites: 5. More data on the nuclides of potassium and noble gases, on exposure ages and meteoroid sizes. *Zeitschrift für Naturforschung* 38a:273–280.
- Voshage H. 1982. Investigations of cosmic-ray-produced nuclides in iron meteorites, 4. Identification of noble gas abundance anomalies. *Earth and Planetary Science Letters* 61:32–40.
- Voshage H. and Feldmann H. 1979. Investigations of cosmic-ray-produced nuclides in iron meteorites, 3: Exposure ages, meteoroid sizes and sample depths determined by spectrometric analyses of potassium and rare gases. *Earth and Planetary Science Letters* 45:293–308.
- Wasson J. T. 1999. Trapped melt in IIIAB irons; solid/liquid elemental partitioning during the fractionation of the IIIAB magma. *Geochimica et Cosmochimica Acta* 63:2875–2889.
- Wasson J. T., Choi B.-G., Jerde E. A., and Ulf-Møller F. 1998. Chemical classification of iron meteorites: XII. New members of the magmatic groups. *Geochimica et Cosmochimica Acta* 62: 715–724.
- Wieler R. 2002. Cosmic-ray-produced noble gases in meteorites. *Reviews of Mineralogy and Geochemistry* 47:125–170.
-